MEASURING THE ERROR BETWEEN ACTUAL AND ESTIMATED ATMOSPHERICS AND THE EFFECT ON ESTIMATING REFLECTANCE PROFILES

Allan W. Yarbrough[a], Michael J. Mendenhall[a], Steven T. Fiorino[b]

Air Force Institute of Technology
Dept of Electrical and Computer Engineering[a]
Dept of Engineering Physics[b]
2950 Hobson Way, Wright-Patterson AFB, OH 45433

ABSTRACT

Accurate target detection and classification of hyperspectral imagery require that the measurement by the imager matches as closely as possible the known "true" target as collected under controlled conditions. Therefore, the effect of the radiation source and the atmosphere must be factored out of the result before detection is attempted. Our objective is to investigate the relationship between uncertainty in the estimation of target spectra and uncertainty in the estimation of atmospherics. We apply a range of atmospheric profiles to a MODTRAN-based prediction of the radiative transfer effect. These profiles are taken from known distribution percentiles as obtained from historic meteorological measurements at the chosen site. We calculate the change in radiative transfer effects as measured by the Euclidean distance, given the range of atmospheric conditions in the historic profile, and show that changes in the atmospheric assumptions change the total transmission, spectral radiance, and estimated reflectance.

1. INTRODUCTION

Atmospheric absorption of electromagnetic energy is a problem across the broader topic of remote sensing. Atmospheric scientists have spent a great deal of effort to characterize the atmosphere, estimate atmospheric parameters from data, and generate methodologies for removing those atmospheric effects (e.g., empirical line correction [1] and MODTRAN [2], to name a few). Although many of the techniques for estimating atmospheric parameters and removing atmospheric effects from imagery have been very successful, there is a level of uncertainty in the estimates that are still unaccounted for on reconstructed data. The misestimation error will have an effect on other processes such as change detection, target detectors such as the Adaptive Matched Filter [3] or Adaptive Cosine Estimator [3], and other algorithms such as the Normalized Difference Vegetation Index (NDVI) [4] used in vegetation health analysis.

This article provides a brief look at how the error in the estimate of the atmospheres affects the reconstruction of a hyperspectral image (i.e., going from sensor-reaching radiance to estimated reflectance and working in the illumination-neutral reflectance environment). To this end, we first investigate and develop a distance measure between atmospheres. This is a non-trivial problem as it is currently unknown what the differences between atmospheric profiles really mean and how two distances with the same numerical value may affect the estimated reflectance of a hyperspectral signature. As such, one must carefully choose how the input error (input being the atmospheric profile) is represented.

The second aspect of this paper is the mapping between input error (how far off is the estimated atmospheric profile from the actual atmospheric conditions under which the targets of interest were imaged) and the output error (the error as measured by the Euclidean distance (ED) between the calculated reflectance spectrum of a target under the true atmospheric profile and that of a target under the estimated atmospheric profile).

2. DISTANCES BETWEEN ATMOSPHERES

There are two general approaches to defining a distance between atmospheres. A first approach is to measure the distance between two solar irradiance curves defined by a blackbody radiator (the sun) transmitting through an atmospheric profile. A second approach is to consider the difference between the profiles themselves. How are atmospheric profiles characterized? The most significant and widely recognized approach is to characterize the atmosphere by its water vapor content, of which several related measures exist.

The fundamental measured quantity of atmospheric water vapor content is the *dew-point temperature* (T_{DP}): the temperature to which a given parcel of air must be cooled at constant pressure for it to reach saturation. From T_{DP}, we can calculate the *vapor pressure* (e_s) – the partial pressure contri-

Thanks to the Air Force Research Laboratory Hyperspectral Exploitation Cell for sponsoring this work. The views expressed in this article are those of the author and do not reflect the official policy or position of the United States Air Force, Department of Defense, or the U.S. Government.

bution of water vapor in a volume or parcel of air – as:

$$e_s(T_{DP}[^\circ C]) = 6.122 \exp\left[\frac{17.67 \cdot T_{DP}}{T_{DP} + 243.5}\right]. \quad (1)$$

The vapor pressure can then be used to calculate both the *mixing ratio* (w) – the mass of water vapor per unit mass of dry air in a given parcel – and the *specific humidity* (q) – the mass of water vapor per unit mass of the moist air parcel – using the following two closely-related formulas:

$$w = \epsilon \frac{e_s}{P - e_s},\ q = \epsilon \frac{e_s}{P - (1-\epsilon)e_s}, \quad (2)$$

where P is the air pressure and in millibars $\epsilon = 0.622$, the ratio of masses for equal quantities of water vapor and dry air (note that since $\epsilon < 1$ and $(1-\epsilon)e_s < e_s$, water vapor is less dense than dry air). The specific humidity can be used to calculate the *virtual temperature* (T_v) – the temperature to which a parcel of dry air must be heated for it to have the same density as moist air at the same pressure – as:

$$T_v = T\left(\frac{1 + \frac{w}{\epsilon}}{1+w}\right) \approx T(1 + 0.6w), \quad (3)$$

where T is the temperature of the moist air parcel. The *air density (ρ)* can then be calculated:

$$\rho = \frac{P}{R_d T_v}, \quad (4)$$

where $R_d = 287 J/kg/^\circ K$, P is in N/m^2, and T_v is in $^\circ K$. We can use the air density to find the *vapor density (ρ_v)*, also known as the *absolute humidity*:

$$\rho_v = \rho q. \quad (5)$$

The transmittance $t(z)$, or the ratio of the radiation reaching the target to the radiation incident on the top of the atmosphere as a function of the target altitude z, depends on both the mixing ratio w and the density ρ as follows:

$$t(z) = \exp\left[-\frac{k_a w \rho H}{\mu}\right], \quad (6)$$

where k_a is the mass absorption coefficient and μ is the cosine of the zenith angle.

We observe from these equations that atmospheric transmission depends on both density and pressure; that these are related to each other by dew-point temperature, atmospheric temperature, and pressure; and that they determine the absolute humidity. We also observe from our meteorological measurements, described in Section 3, that variations in dew point and temperature are themselves highly correlated with each other.

We describe the distance between atmospheres using the ED between water vapor measurements taken at four radiosonde layers. In particular, we consider the dew point temperature (in ^oC), water vapor mixing ratio (in grams of H_2O per kilogram of all other gasses), absolute humidity ρ (grams of H_2O per cubic centimeter), and air density (in kg_{air}/m^3; note that moist air is less dense than dry air) as independent measures of water vapor content. We also use the ED to describe the distance between spectral measurements taken at 887 frequencies between $3984 - 27020 cm^{-1}$ by transmission (t), reflectance (r), and sensor reaching radiance (R_{sr}). The formula for the ED is shown in Eqn. 7, where m is the measure of water vapor content as a function of radiosonde layer z_i and atmospheric profile a_j, where $\{a_1, a_2\}$ are the two atmospheric profiles being compared. Preliminary results are presented in Section 4 using this methodology.

$$\begin{aligned} d(a_1, a_2) &= \sqrt{\sum_{i=1}^{4} \left(m(a_1, z_i) - m(a_2, z_i)\right)^2} \quad (7) \\ m &\in \{T_{DP}, w, \rho, \rho_v, t, r, R_{sr}\} \end{aligned}$$

3. EXPERIMENTATION

The atmospheric profile data are taken from the Laser Environmental Effects Distribution Reference (LEEDR) [5]. These data were collected from meteorological measurements at multiple sites across the world. They are grouped by the month, time of day, and - most significantly - the percentile in which they fall in a distribution correlated to relative humidity. For the purposes of this paper, we consider atmospheric profiles taken at nine different percentiles of the distribution: 1%, 5%, 10%, 20%, 50%, 80%, 90%, 95%, and 99%. The seasonal, geographic, and time-of-day parameter variations contained in the LEEDR database are based on meteorological measurements and atmospheric boundary layer characterizations at four atmospheric levels: the surface; 500m above ground level (AGL); 1000m AGL; and 1500m AGL. Significantly, over half of the water vapor in the entire atmosphere is below 1500m in altitude. We observe from these measurements that as water vapor content increases, the atmospheric temperature also increases. This tends to prevent an easy analytical generalizations based on Eqn. 6, instead requiring the use of the experimental data.

The profiles taken at these distributions become user-defined atmospheres used by MODTRAN [2] to generate the sensor-reaching radiance for a target of a spectrally independent surface albedo of one. The scene geometry is of a sensor at 3048m AGL with a nadir zenith angle imaging a target on the surface at 300m MSL. The image is collected at 1:00 p.m. EDT on June 1, 2001 at a location of 43°E, 77°W. The MODTRAN parameters include modeling multiple scattering with $8\times$ DISORT, no aerosols and MODTRAN-calculated visi-

bility (IHAZE = 0, VIZ = 0). For the no-aerosol case, the differences between the spectra are small, yet measurable; greater differences can be obtained by including aerosols and limited-visibility conditions. We repeat the simulation for four standard MODTRAN surfaces: cropland, deciduous trees, galvanized pipe, and olive paint. The reflectance spectra corresponding to these surfaces are shown in Fig. 1.

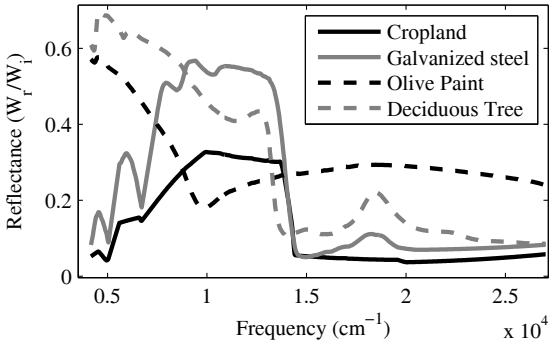

Fig. 1. Reflectance plots of four target signatures.

4. RESULTS

Results are presented in Fig. 2, 3, and 4, where the *x*-axis is the ED between the atmospheric profile, as defined by water vapor content, as it appears in the $1st$ percentile ("most dry") of the distribution and all higher percentiles of that distribution. Note that the *x*-axis is labeled by percentile rather than by the ED values themselves. In Fig. 2, the *y*-axis is the ED between the total atmospheric transmittance – from the top of the atmosphere to the target to the sensor – as simulated under the $1st$ percentile atmosphere and those simulated under all other percentiles. In Fig. 3, the *y*-axis is the ED between the "true" target reflectance (again using the $1st$ percentile of the distribution as the baseline) and its reflectance as estimated under atmospheric profile assumptions based on other percentiles of the distribution. In Fig. 4, the *y*-axis is the ED between the radiance reaching the sensor as reflected by the target as simulated under the $1st$ percentile and all other percentiles. While our initial examination included varying the choice of the percentile chosen as the baseline, we discovered that the shape and scale of the resulting relationship was largely independent of that choice. Fig. 3 and Fig. 4 also show the effect of targets with non-uniform emissivity.

Several generalizations can be made from these relationships. Controlling for choice of vapor content measure (i.e., dew point, mixing ratio, absolute humidity, and density), the relationship between atmospheric transmission, estimated target reflectance, and sensor reaching radiance is linear. This validates our expectation that the contribution of atmospheric emission to sensor reaching radiance is negligible; thus, the sensor reaching radiance is approximately the product of the

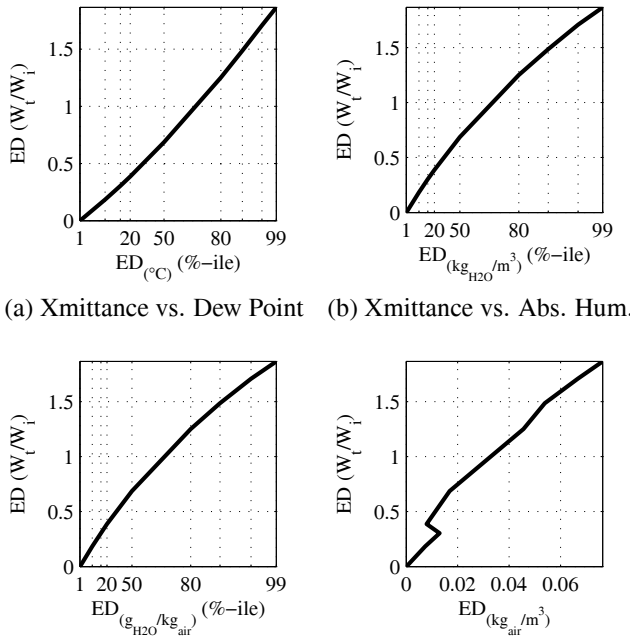

(a) Xmittance vs. Dew Point (b) Xmittance vs. Abs. Hum.

(c) Xmittance vs. Mixing Ratio (d) Xmittance vs. Density

Fig. 2. Plot of the ED between atmospheric water vapor content profiles (x-axis) and the EDs between total atmospheric transmittances as modeled under those profiles (y-axis).

constant solar radiance and the atmospheric transmission for a given target; the target reflectance, in turn, is obtained from the ratio of sensor reaching radiances for the different atmospheres. We also see that the relationship between the absolute humidity and water vapor mixing ratio is also linear; as indicated by Eqn. 3, this is expected for $w << 1$.

The relationship between the ED of the estimated target reflectances (Fig. 3) and sensor reaching radiances (Fig. 4) and the various measures of atmospheric distance, while highly linear, are also highly target-dependent for the amount of change in radiance distance a given atmospheric distance will cause. In general, we can see from Table 1 that the higher the overall radiance energy from a particular target (as measured by the magnitude of the radiance scaled by the spectral resolution), the greater the slope of the plot.

Target	Spectral Energy ($\mu W/cm^2/str$)
Cropland	8.3101
Deciduous Tree	14.505
Galvanized Metal	12.392
Olive Paint	14.511

Table 1. Table of Spectral Energies (magnitude scaled by the spectral resolution) of four targets signatures.

Otherwise, we see that while all relationships are highly correlated, they vary subtly depending on the choice of water vapor measurement. Mixing ratio and absolute humidity

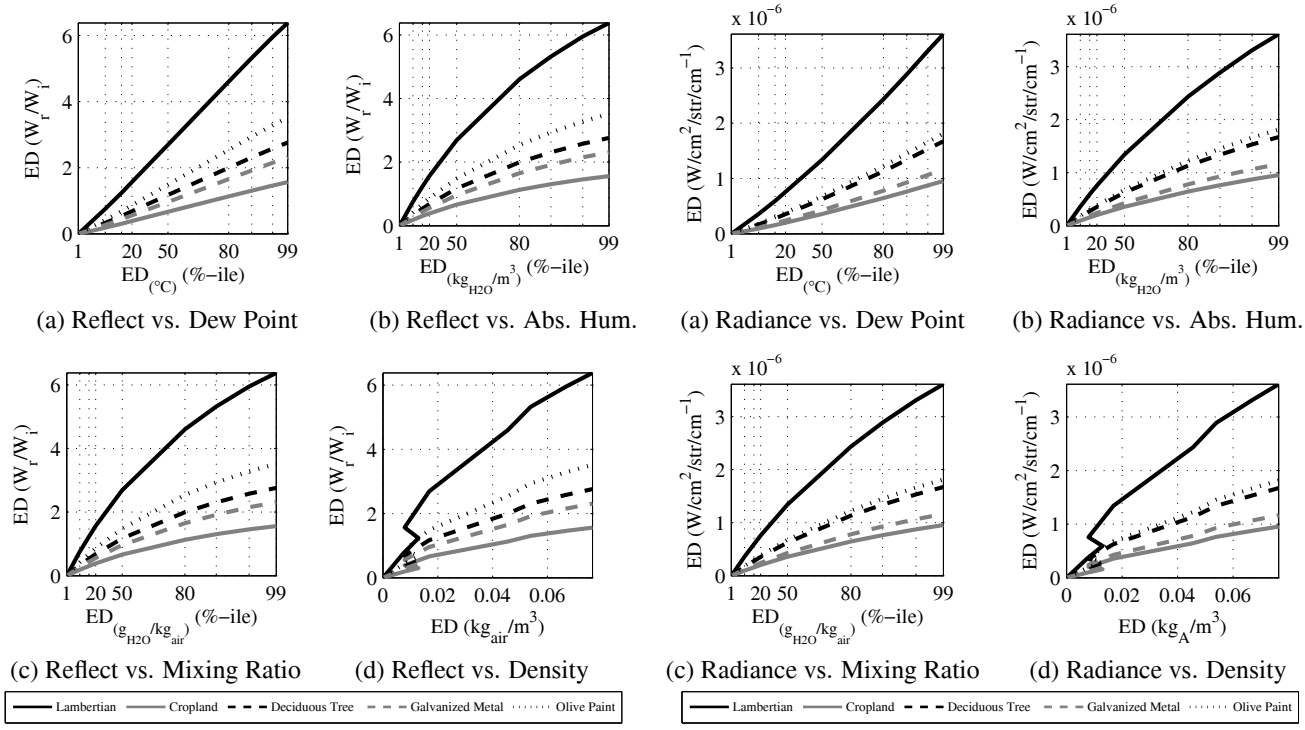

Fig. 3. Plots of the EDs between the 50th percentile atmospheric profiles and the other eight profiles (x-axis); and the corresponding ED between the estimated reflectance spectra for a target of uniform emissivity (y-axis).

Fig. 4. Plot of the ED between the 1st percentile atmospheric profile and the other eight profiles (x-axis) versus the corresponding Euclidean Distances between the sensor reaching radiance spectra for a target of uniform emissivity and four MODTRAN-defined targets (y-axis).

show a exponentially diminishing relationship with radiance, as would be predicted by the derivative of Eqn. 6 with respect to $w\rho$. Dew point shows a near perfect linear relationship. Density shows a noticeable discontinuity between the $10th$ and $20th$ percentiles; this reflects the decrease in the recorded temperature data corresponding to these percentiles in what is otherwise a positive correlation with relative humidity.

5. CONCLUSIONS

Our analysis shows a highly correlated relationship between atmospheric distance and spectral distance as measured by the ED between percentiles of the measured distribution of atmospheric profiles at a given site. It further shows that the reflectance spectrum of the target helps determine how much spectral error a given atmospheric error will introduce. An area of further research will be to consider the visibility-limiting effects of aerosols as a function of surface humidity and how they change the amount of spectral variation in MODTRAN simulations.

6. REFERENCES

[1] E. Karpouzli and T. Malthus, "The empirical line method for the atmospheric correction of IKONOS imagery.," *International Journal of Remote Sensing*, vol. 24, pp. 1143 1150, 2003.

[2] A. Berk and G.P.; Acharya P.K.; Robertson D.C.; Chetwynd J.H.; Adler-Golden S.M. Bernstein, L.S.; Anderson, "MODTRAN cloud and multiple scattering upgrades with application to AVIRIS," *Remote Sensing of the Environment*, vol. 65, pp. 367–375, 1998.

[3] D. Manolakis and G. Shaw, "Detection algorithms for hyperspectral imaging applications," *IEEE Signal Processing Magazine*, vol. 19, no. 1, pp. 29–43, Jan 2002.

[4] J. E. Colwell, "Vegetation canopy reflectance," *Remote Sensing of the Environment*, vol. 3, no. 3, pp. 175183, 1974.

[5] S.T. Fiorino, R. Bartell, M. Krizo, G. Caylor, K. Moore, T. Harris, and S. Cusumano, "A first principles atmospheric propagation and characterization tool: the laser environmental effects definition and reference (LEEDR)," in *SPIE Proceedings*, Feb 2001, vol. 6878, pp. 122–124.